Silicon (2022) 14:11417–11427
https://doi.org/10.1007/s12633-022-01751-2

ORIGINAL PAPER

The Fabrication of High-Anisotropy Silicon Nanowires Based on MACE Method for Photonic Sensor

A. Mohamedyaseen[1] · **P. Suresh Kumar**[2]

Received: 27 December 2021 / Accepted: 6 February 2022 / Published online: 11 April 2022

Abstract
Future electronics will be made of silicon nanostructures (SiNs). Mechanical, electrical, and optical characteristics, as well as litho resistivity and thermoelectricity, making them remarkable multi-functional materials. SiNs are used in nanoelectronics, nanoresonators, light-emitting diodes, nanosensors, and thermoelectric energy scavengers, to name a few. Mechanical properties of SiNs, which are expected to differ from those of bulk SiNs, are crucial to the performance and dependability of these nanoelectronics. The metal-aided etching procedure was employed to make the SiNs used in this investigation. This SEM picture of as-grown SiNs displays its structure and demonstrates that the Ns have widths of less than 100 nm. The X-ray diffraction pattern of SiNs reveals the Ns' single-crystalline structure. When polarization-resolved reflections were used on these nanowire arrays, the reflection properties of s- and p-polarized laser beams were found to differ significantly. The findings of this study can be used to a wide range of optical devices that utilise SiNWs, including photodetectors and solar cells. Furthermore, it has the potential to be beneficial in medical imaging.

Keywords Silicon · Electro less Chemical Etching · Nanowires · MACE · SiNW · XRD · Bulk SiNs

1 Introduction

Lilienfeld was the first to get a patent on the field FET concept, which occurred in 1930. It was the realisation of the Si-SiO_2 structure [1] that paved the way for widespread commercial application beginning in 1960. Integrated circuit technology has advanced significantly in the forty years that have elapsed since then. Electronic gadgets have undergone continuous improvement in terms of device density and clock rate [2]. Observing Moore's law of exponential growth has been a long-standing commercial trend for many decades. This remarkable breakthrough in semiconductor electronics was built on the reduction in the size of silicon MOSFETs, which allowed for an increase in the density of logic and memory chips. It is anticipated that semiconductor technology will continue to improve tremendously in the near future, according to the International Technology Roadmap for Semiconductors (ITRS) [3].

Despite Intel's recent demonstration of 22 nm technology, it is still unknown whether the trend will continue beyond the 10 nm frontier. This is despite the fact that the technology showed promise to stay up with Moore's law. It is physically conceivable to shrink the gate length of silicon field-effect transistors (FETs) to as small as 10 nm in their advanced (ultra-thin-channel, double-gate) configuration [4]. The nanoscale properties of devices get more diverse as they go smaller, including the threshold voltage and on/off current, which can have a substantial impact on the performance of the device. Because of these more severe technological and basic restrictions, traditional scaling procedures, which maintain the device's essential structure while shrinking its size, are put to the test [5].

A new generation of one-dimensional (1D) structures, including carbon nanotubes (CNTs) and semiconductor nanowires, has been developed in response to the predicted limitations of photolithographic technology and in order to sustain the historical scaling trend in semiconductor technology (NWs) [6]. The relevance of these components arises from the fact that they can function as both active devices and interconnects, allowing them to perform two of the most

✉ A. Mohamedyaseen
mohamedyaseenece@gmail.com

[1] Department of ECE, Excel Engineering College, Namakkal, India

[2] Department of EEE, Mahendra Engineering College (Autonomous), Namakkal, India

critical functions of a nanosystem at the same time. Therefore, it is possible to accurately control the critical device size down to the atomic scale during the growth process. Even though researchers have been working on complex arrays of nanotube devices uninterrupted for some years, no practical methods for building them have been discovered yet.

The classification of nanomaterials based on their size is depicted in Fig. 1. The development of many nanostructured materials has occurred throughout the previous few decades [7].

When nanostructured materials are viewed under a microscope, the effects of size dependency can only be seen in one direction because they are all made up of sub-micron or nanoscale building blocks [8]. As a preliminary stage, materials with nanoscale structure are categorised in this way.

A billionth of a unit of measurement is referred to as "nano" (10^{-9} m). Nanostructured materials with zero dimensions are zero-dimensional materials themselves [9]. Because of their small size, nanoparticles are the most frequent way to display zero-dimensional nanomaterials. These zero-dimensional materials have been studied extensively in a number of applications, including LED solar cells, single electron transistors, and lasers [10].

One-dimensional nanomaterials are materials that do not have a limit to their size at the nanoscale. For example, one-dimensional nanostructured materials are ideal platforms for researching a wide range of novel phenomena at the nanoscale, and they are also being used to investigate the relationship between functional proportion and dimensionality in nanoscale materials [11]. Among the one-dimensional nanomaterials are nanowires, nanorods, nanotubes, and nanoribbons, among other things.

When both dimensions are more than or equal to the nanoscale range, this sort of material is referred to as two-dimensional. This type of 2-D NSMS has a plate-like shape and integrates nanofilms, layers, and nanocoating's into its construction [12]. In recent years, there have been several advancements in the chemical composition of 2-D NSMs that allow them to be either amorphous (or) crystalline in structure. In recent years, there has been a lot of interest in 2D nanomaterials, which have features that are depending on their geometry. A two-dimensional NSM is defined as a structure that is branched, prismatic, or plate-like [13, 14].

A three-dimensional nanomaterial is a bulk nanomaterial that is not restricted to the nanoscale in any dimension of the material and is therefore not classified as such. These materials have three arbitrary dimensions that are more than 100 nm in length, and each of these dimensions is different [15]. The quantum size effect causes three-dimensional nanostructured materials to have a higher surface area than bulk materials as a result of their smaller size. Three-dimensional nanostructures can be used to create magnetic materials, electrode materials for batteries, and other catalytic materials [16–18], among other things. Many other types of 3D nanomaterials can be constructed from dispersed nanoparticles or nanotube bundles, for example.

2 Literature Survey

Ruby A. Lai el al., [19] proved, using metal-assisted chemical etching, that the schottky junction formed between metal and silicon plays a crucial role in the distribution of holes into silicon caused by an oxidising agent such as hydrogen peroxide, according to their findings. They discovered that their proposed mechanism may be used to explain how factors like as doping amount, doping type, crystallographic surface, etching direction, and etching solution composition all influence the pace at which etching takes place.

R.F. Balderas et al., [20] used metal-assisted chemical etching to create sensors based on porous silicon, which they patented. Using hexagonally oriented porous silicon (PSi) pillars with large pores on top of porous silicon (PSi) pillars

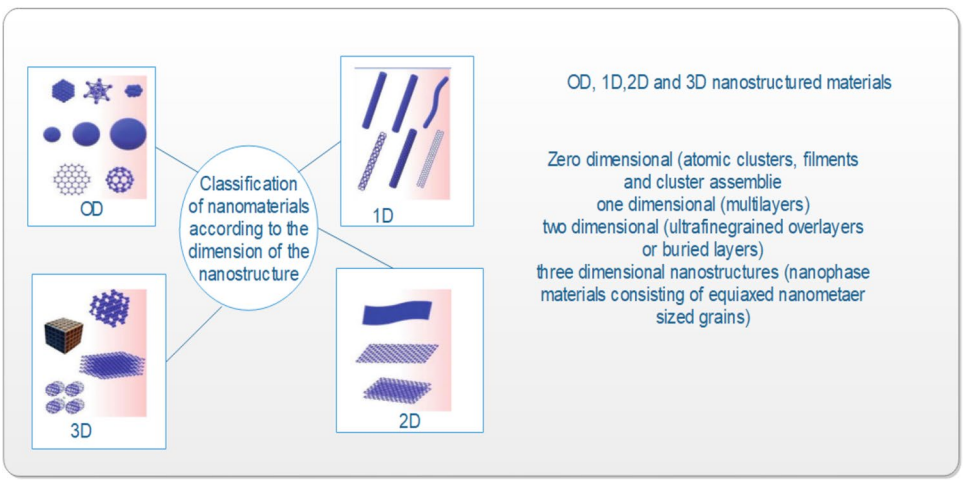

Fig. 1 Classification of dimensions based Nano Materials

with smaller pores, porous silicon (P Si) sensors were produced in this study. These structures were created using a combination of techniques including colloidal lithography, gold film deposition, and MACE. The variable pore widths in MACE can be obtained by modifying the etching solution used in the process. They came to the conclusion that the reflectance spectrum of the sensors had the complex interference pattern that had been predicted. Protein A and sucrose, as well as other smaller biomolecules, were revealed to be capable of penetrating the PSi barrier.

Lingyu Kong et al., [21] conducted an examination into the transport channels that are responsible for metal-aided chemical etching of silicon. When using metal-assisted etching, metal ions are responsible for the oxidation of silicon and the transfer of hole charges in the etching solution. For catalyst films with a thickness less than 30 nm, holes and cracks are employed to transport chemicals and byproducts through the catalyst film as it is being etched. When the thickness of the metal/silicon interface exceeds 30 nm, transport occurs at the interface. It was their goal to demonstrate that ion transport has a major advantage over carrier transport at the catalyst-silicon interface in this experiment.

3 Background

In addition to exhibiting a wide range of intriguing optical, electrical, magnetic, mechanical, and other properties, metal oxide nanostructures are among the most interesting functional materials, as previously stated [22–25]. In addition to self-cleaning and surface enhanced Raman spectroscopy (SERS) molecule identification, self-cleaning metal oxide nanostructures have the potential to be used in cosmetics, catalysis, medical diagnostics, and a variety of other applications [26–28]. Magnetic and optical devices, as well as batteries, screens, and fuel cells, are examples of such devices.

Since silicon (Si) is readily available and non-toxic, it has a long shelf life and is highly stable. Its electrical characteristics can be tuned, and it has a high photoelectric activity, making it a popular choice for energy and electronic devices. Silicon's characteristics can be improved through the use of nanoscale engineering. Because of its one-dimensional (1D) morphology and nanoscale diameter, silicon nanopores, nanowires, nanorods, and nano tubes can be used in energy and flexible electronics [24]. Significant investigation has been conducted into the unusual properties of silicon nanostructures, such as quantum size effects and high surface-to-volume ratios, throughout the last several decades. There are many different shapes and sizes of SiNs, but the two most prevalent are spherical and cylindrical.

- Silicon nanowires
- Porous silicon

Devices based on the physical properties of silicon nanowires are the focus of our research. Figure 2 illustrates the various uses of SiNs.

4 Methodology

Physical, chemical, electrical, and magnetic properties of nanoscale-structured materials differ considerably from those of bulk materials, as do their electrical and magnetic properties. Materials with nanostructures. As a result, they've developed a strong desire to learn more about scientific and technological topics [19]. Nanomaterials can be created in a variety of ways utilising a variety of techniques. The manufacturing process for nanomaterials is depicted in Fig. 3. The development of nanoparticles is being improved through the use of physical and chemical processes. Physical and chemical sciences can benefit from the use of top-down and bottom-up approaches to problem solving. It is feasible to obtain nanostructures via a top-down approach by first regulating macroscale structures and then manipulating nanoscale structures. Nanostructures are formed through the bottom-up miniaturisation of components and the self-assembly of components in a controlled environment.

In this study, aqueous etching (also known as electroless chemical etching) is employed to fabricate Si nanowires. A number of chemicals and materials are used in this process, including silicon wafer, hydrogen peroxide, $AgNO_3$, and H_2O_2. First and foremost, cleaning must be accomplished. A thin layer of deionized water is carefully applied to the substrate. The following step involves cleaning the wafer

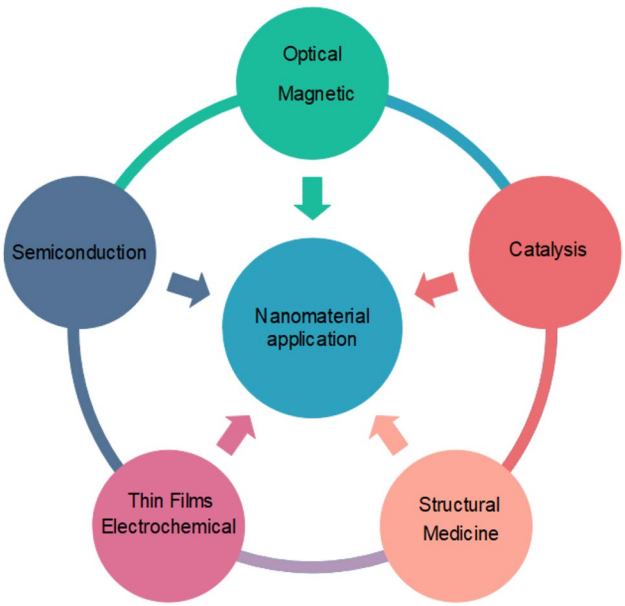

Fig. 2 Application of the silicon nanowires

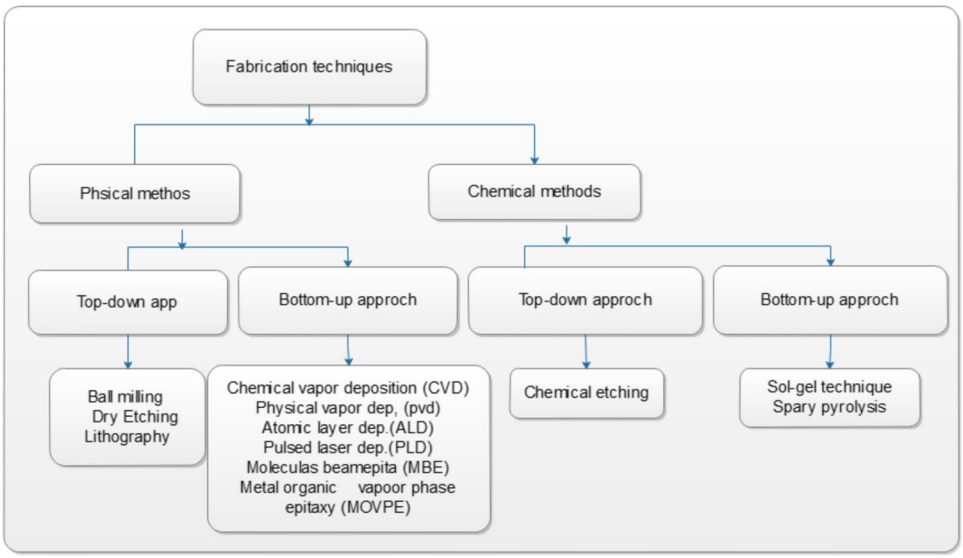

Fig. 3 Fabrication techniques

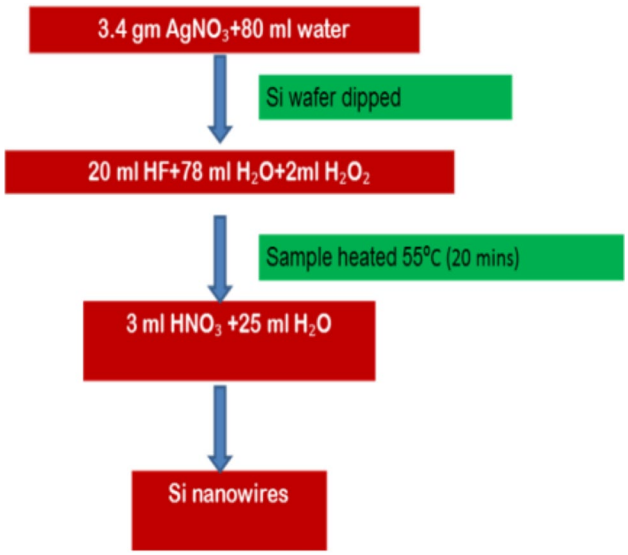

Fig. 4 Fabrication of Silicon nanowires

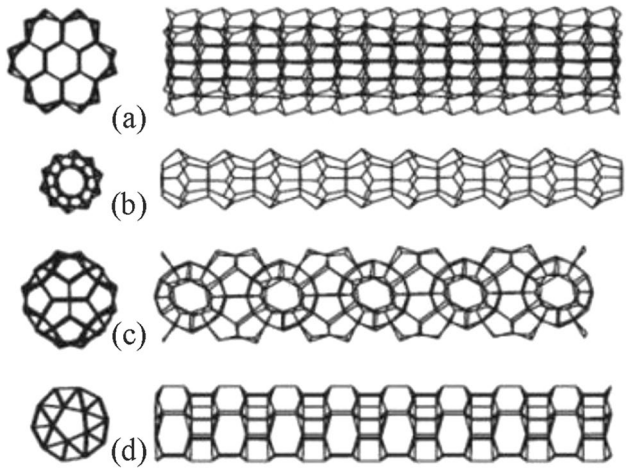

Fig. 5 Schematic representation of Silicon Nanowire

using isopropanol alcohol. The wafer is cleaned with isopropanol alcohol before being rinsed with HF at a concentration of 5%. We went through all of these stages in order to get rid of dust, organic matter, and other pollutants. After the substrate had been carefully cleaned, the glass beakers and Teflon that were utilised in the fabrication process were extensively cleaned as well. 80 mL of water were treated with 3.4 gm of $AgNO_3$, and 20 mL of HF were added to make a final volume of 80 ml of water Finally, after three seconds, the Si wafer was removed from the solution [20]. Other silicon wafers were subjected to the same technique. Figure 4 depicts fabrication of Silicon nanowires.

Many distinct types of structures for SiNWs have been observed and described. Structures such as clathrates, tetrahedral structures, and polycrystalline nanowires are all examples of these types of materials. SiNWs' surface is easily oxidised in air due to the high density of dangling bonds present on the surface of the nanowires. When it comes to SiNWs, electrical carriers can only travel in one direction. When compared to bulk silicon, the physical properties of crystalline silicon are significantly different. Figure 5 represents schematic representation of Silicon Nanowire.

5 Process of Chemical Etching

This method's usual procedure and basic mechanism are represented in Fig. 6 after a simple deposition of metal on a Si substrate and immersion in an acidic solution that contains both hydrogen peroxide (HF) and an oxidising agent (e.g.,

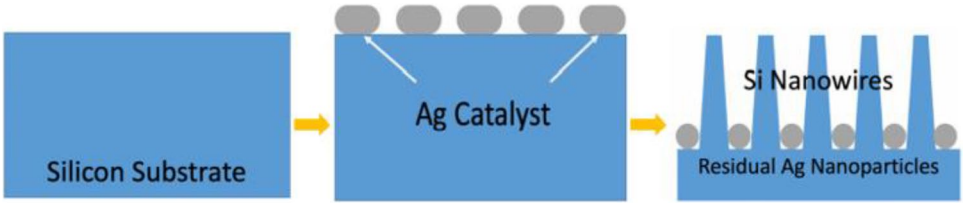

Fig. 6 Process of chemical etching

sulfuric acid). As a result of the anisotropic dissolving of Si, nanowire structures are left on the surface of the substrate. Metal acts as a catalyst to accelerate chemical etching by preferentially transporting metal atoms along the crystallographic direction of the silicon crystal. With regard to SiNW crystals, they share a crystal axis with their source wafer and have the same doping type and level [2], which is consistent with their source wafer [21]. In any chemical laboratory, the remainder of the fabrication process can be carried out at room temperature and in an ambient atmosphere, without the need for a furnace or specialised equipment such as sputtering or electron beam evaporation.

Metal aided chemical etching, a straightforward and low-cost approach for fabricating silicon nanowires, has been developed (MACE). Metal aided chemical etching processes [73] can only be used to facilitate the etching of Si when noble metals (Pt, Au, Ag, and Pd) are used as catalysts. It has long been recognised that chemical reactions occur more frequently in the vicinity of noble metals than in other locations. Because of its simplicity, low cost, ease of process control, and reproducibility, it is projected that MACE will be used more frequently as a dependable strategy for generating Si nanostructures in the future. MACE is classified into two types: one-step MACE and two-step MACE. In MACE, the deposition of metal nanoparticles catalyses non-uniform etching of silicon in an aqueous etching solution, which results in the formation of microstructures. SiNWs are produced directly from the silicon substrate in the MACE process. This method makes it simple to achieve optical and electrical characteristics that are flexible. The mechanism of MACE is well depicted in Fig. 7. During the complex metal catalysed process known as MACE1, there is just one phase that takes place (one step MACE). During the process of oxidation and dissolution of silicon, metal nanoparticles (with Ag serving as the noble particle) are reduced in concentration.

In the chemical reaction that takes place in the etching solution, there are two steps that need to be completed: HF and $AgNO_3$. According to Eq. (1), during the reaction between HF and $AgNO_3$, the valence bond of silicon is grabbed by the Ag + ions and transformed to Ag^0 (1). Under the influence of the Ag^0 nucleus, it is oxidised to SiO_2 (Eq. 2) and then dissolved by hydrofluoric acid (eq 0.3). When SiO_2 dissolves, a void is generated, and the Ag nucleus falls into this vacancy.. Because of the oxidation, there are more electrons in the solution, which attracts more Ag + ions, which in turn drives the pits to grow Ag nuclei. The reaction mechanism of MACE is depicted in the diagram below.

$$\mathrm{Ag} + (\mathrm{aq}) + \mathrm{e} - \mathrm{VB}, \mathrm{Si} \rightarrow \mathrm{Ag0} \quad (1)$$

$$\mathrm{Si(solid)} + 2\mathrm{H2O} - 4\mathrm{e} - \mathrm{VB}, \mathrm{Si} \rightarrow \mathrm{SiO2(Solid)} + 4\mathrm{H+} \quad (2)$$

$$\mathrm{SiO2(Solid)} + 6\mathrm{HF} \rightarrow \mathrm{H2SiO2} + \mathrm{H2O} \quad (3)$$

Describes a process for controlling and manufacturing advanced NWs structures that uses metal-assisted chemical etching (MACE) to control and create the structures. It is possible to fabricate anisotropic high aspect ratio semiconductor nanostructures using the wet-etching method MACE while avoiding damage to the lattice. An etching procedure

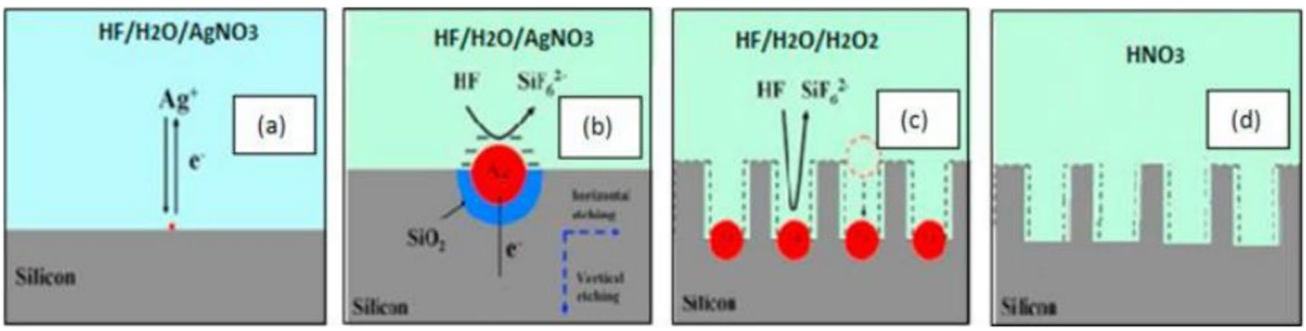

Fig. 7 Mechanism of Metal Assisted chemical etching

with no variation in the z direction can be used to manufacture the suggested quad-crescent design in a single step, and this can be accomplished in a single step. Metallic particles with specific shapes and periodicities can be etched into the semiconductor NW in a controlled manner. It is necessary to follow the strategies shown in Fig. 8 sequentially in order to construct the proposed structure. After cleaning the Si substrate using ethanol and acetone, the surface is polished to a smooth finish.

A bottom contact of Ag is coated on the Si substrate with the use of thermal evaporation. The glancing angle deposition approach can also be used to create the intended crescent shape, as shown in the image below. Techniques for creating crescent designs include reactive ion etching, electron beam lithography, and holographic lithography, to name a few. According to the demonstration in step 4, the Si substrate is etched until the desired length is reached. The etching procedure, which employs a mixture of hydrogen peroxide (H_2O_2) and hydrochloric acid as a final step, is used to remove the mask layer from the surface (HCl). The periodic array of the optimised QCr-NW structure is depicted in Fig. 8 (e). The proposed design differs from the previously developed NWs in the shapes of nanopyramid, nanocone, and nanofunnel that have been previously developed.

6 Results and Discussion

According to the authors of the aforementioned paper, only a few research have been conducted simultaneously on the mechanical, morphological, and optical features of silicon nanostructures (SiNs). All of these findings, taken together, contribute to a better understanding of the basics of the SiNs that have been generated and their mechanical reactions. The findings of this study may be useful in continuing the development and improvement of SiNs' use in a variety of electrical and thermoelectric applications, as well as in other fields.

In this work, to produce super continuity, we used a wavelength range of 0.8 to 1.7 nm and a core diameter of 420 to 480 nm. This research is motivated by high mode confinement within the core, low dispersion, and strong nonlinearity. Figure 9 shows the mode field distribution for a laser with a wavelength of 0.8 m and a core diameter of 480 nm. Finite element methods are used to calculate the fundamental mode's effective refractive index.

Both the total reflected intensity (p/s) for each of the two distinct array sizes is depicted in Fig. 10. Between 450 and 600 nm, a polarization-independent reflection peak is found. The peak changes somewhat to longer wavelengths for both polarizations as the diameter increases, resulting in lower reflection intensities at higher wavelengths. Contrary to expectations, as silicon volume grows, this is the opposite. In addition, the s-polarized input has higher reflection intensities than the p-polarized input. Due to the sample's structure, the air-SiNW interface and SiNW-silicon contact generate numerous reflections that may interfere constructively or destructively when the input wavelength changes. Figures (Fig. 10) for both polarizations show theoretical reflections from the air-silicon contact for comparison. In comparison to silicon, the reflection from the SiNW arrays is quite different. S-polarized beam reflection decreases with increasing SiNWs, yet p-polarized beam reflection increases with increasing wavelengths larger than 400 nm. Figure 10 demonstrates that there are

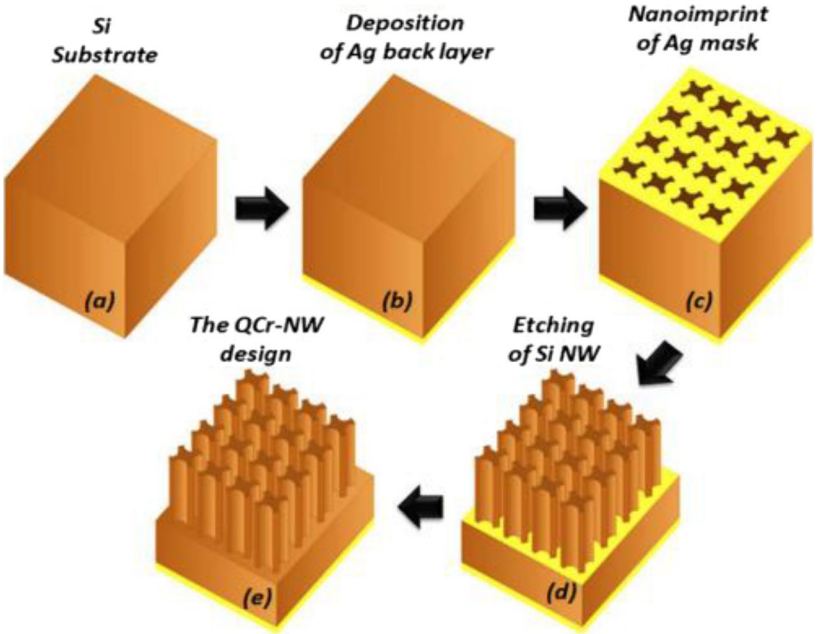

Fig. 8 Fabrication steps for the MACE reported crescent Si-NW structure

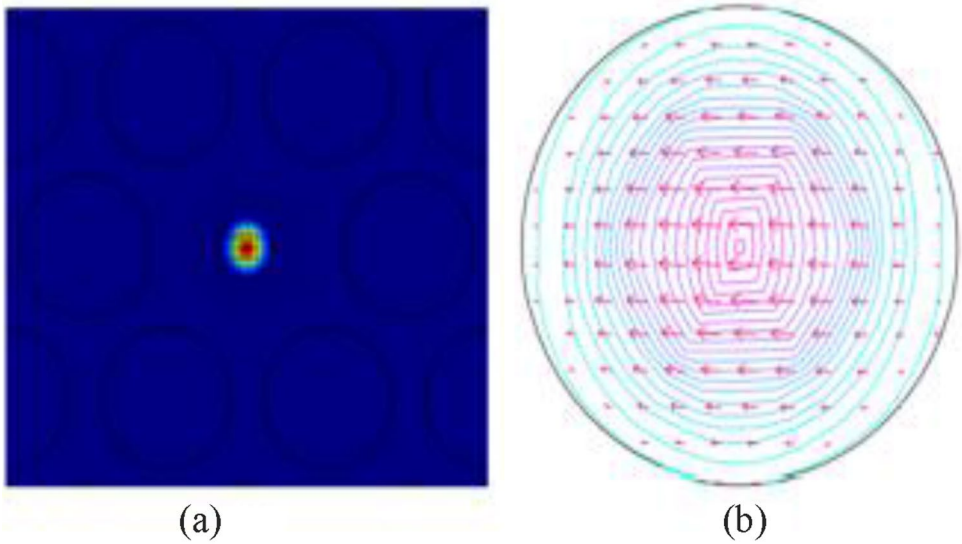

Fig. 9 Mode field distribution for a laser with a wavelength of 0.8 m and a core diameter of 480 nm

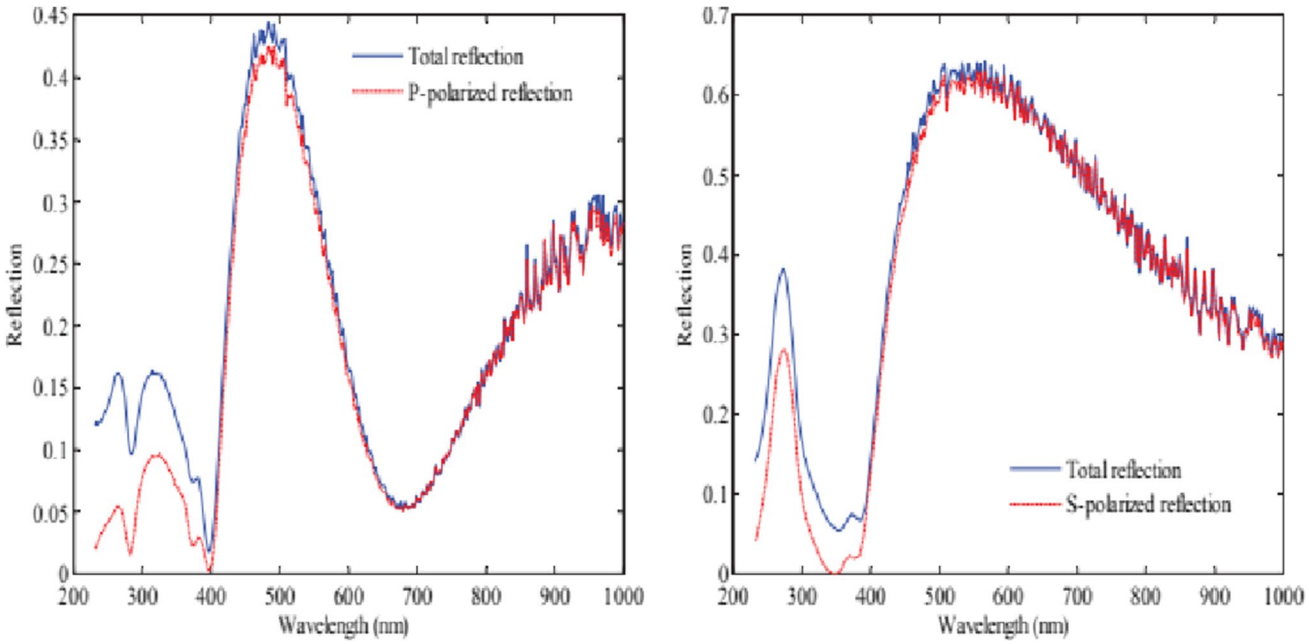

Fig. 10 p and s polarised inputs

wavelengths where the reflection is greatly reduced, and these troughs are dependent on the object's diameter.

Instantaneously following the application of the Zn layer, it became completely opaque. In contrast to ZnO/Zn thin films, which exhibit high transmission and a prominent absorption edge in the UV area (Fig. 11(a)), ZnO thin films exhibit good transmission and a pronounced absorption edge in the visible region (Fig. 11(b)). In the presence of free electrons discharged from the Zn contact, electrons accumulate in the ZnO conduction band, resulting in a bleaching of the excitonic feature in the ZnO conduction band.

A trapping of electrons occurs at the ZnO/Zn interface, as illustrated in Fig. 11(a), enhancing the absorption of ultraviolet and far infrared light while concurrently increasing the dipole moment. Recently, it was demonstrated that organic semiconductors can trap light for the first time in their history. Consequently, the formation of a dipole layer between Zn and ZnO is thought to be responsible for the production of 'effective n-type' doping.

The photoluminescence characteristics of silicon nanostructures were examined at wavelengths ranging from 350 to 1000 nm using an Ocean Optics USB 4000-VIS–NIR detector and a 375-nm laser (5 MW), both of which operated

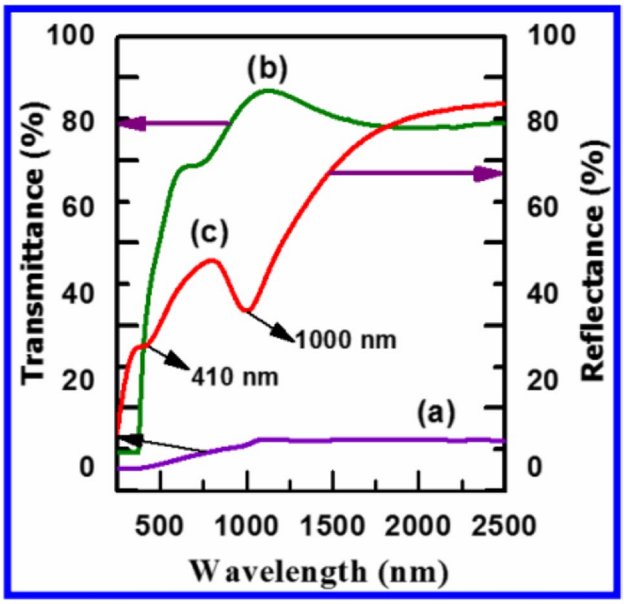

Fig.11 Transmittance analysis based on different etching periods

in Continuous Wave (CW) mode. The presence of F-band luminescence in porous Si after ageing was discovered, and the—transitions in Si nanocrystals were found to be responsible for this. On the other hand, as illustrated in Fig. 12, the PL spectra of silicon and silicon nanostructure are visible.

An excitation peak at the band edge of ZnO/Zn thin films exhibits a relative red shift when compared to the rest of the film (Fig. 13). Lower-wavelength excitation properties of both thin films (at 338 nm and 316 nm, respectively) are, on the other hand, substantially unaltered at these shorter wavelengths. Two separate processes are responsible for the PLE resonance observed here, as proven by the findings.

The bands are detected in both ZnO and ZnO/Zn films when PLE is used to measure green, red, and blue emission. The disordered array was created using nanowires with 30–80 nm diameter. As a result of van der Waal interactions, nanowires clustered randomly. The substrate for both samples was a Si wafer. It is shown in Fig. 14 that the nanowires have been etched. Each of the nanowires had a length of 650 nm and a pitch of 100 nm. The square lattice of organised nanowire arrays stood nearly vertically above the array. Some of the nanowires with a smaller diameter were bundled together, resulting in the disordering.

Figure 15 depicts the testing flowchart. We could measure the PL for various excitation and emission polarizations since we employed two polarizers. When measuring emission, we focused on a beam with an angle of 30 degrees for both the beam's direction of travel and its measurement axis. Because the electric field of the s-polarized input beam was perpendicular to the nanowires, the polarisation was also perpendicular. An electric field perpendicular to the nanowires is one component of the p-polarized beam. Non-polarized light can be used to create highly polarised

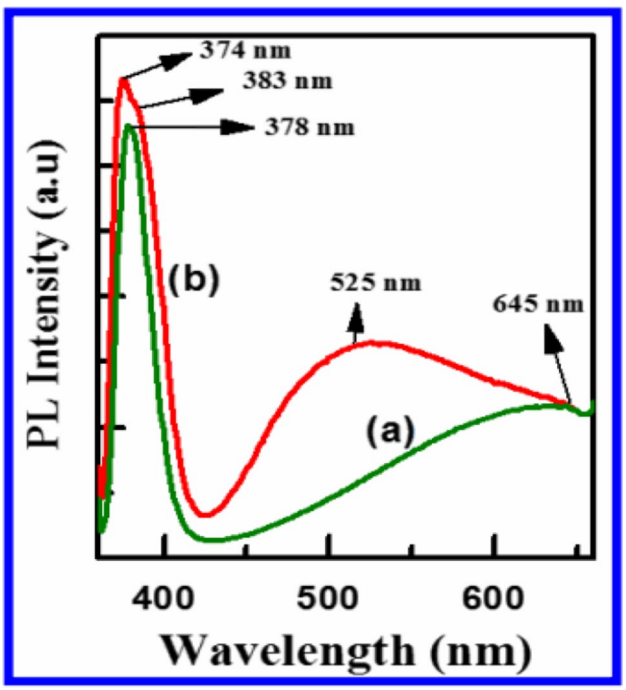

Fig. 12 Photoluminescence Analysis based on different etching periods

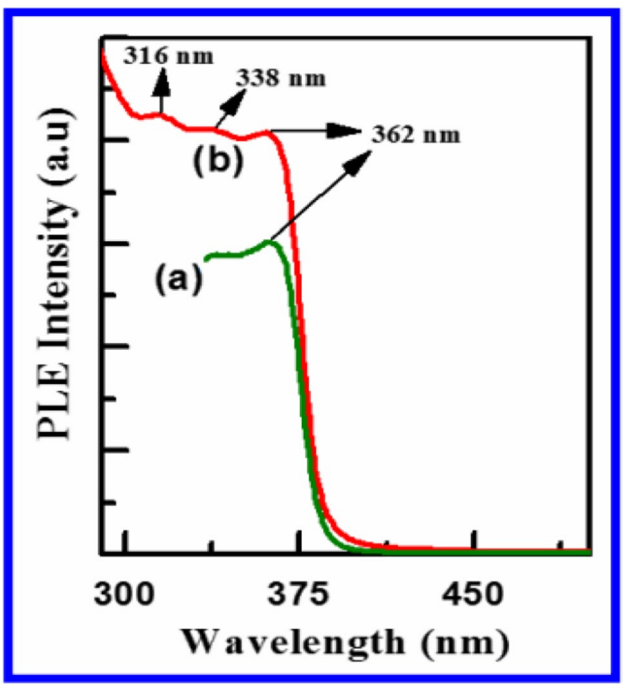

Fig. 13 Silicon nanostructure with Ag sample for different etching time periods

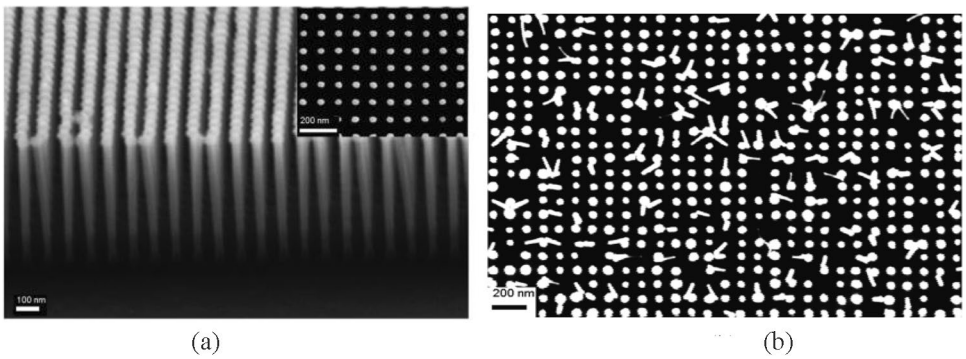

Fig. 14 (a) SEM image showing ordered array of etched nanowires. (b) SEM image of the etched nanowires in the disordered array

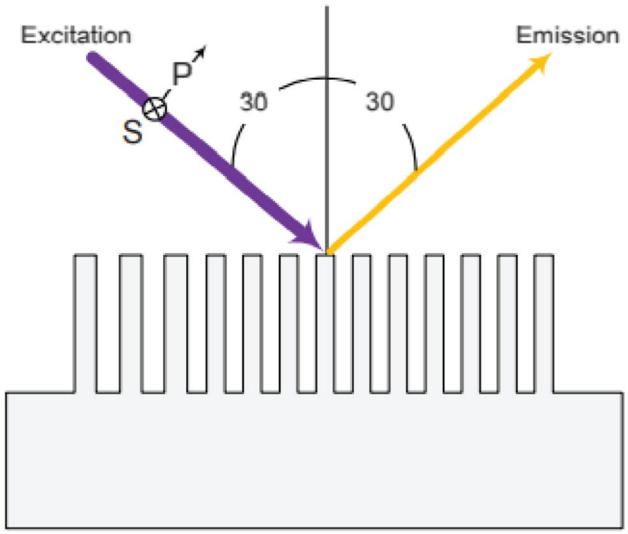

Fig. 15 PL Measurement Schematic

fields within a nanowire with a high refractive index contrast. Because of the nanowire's short wavelength, the field is expected to be stable.

Figure 16 shows that PL emission occurred in both the s- and p-polarizations when nanowires were activated by either a p-polarized or an s-polarized beam. According to the table, the output polarisation with the highest emission has the maximum emission for both the input and output polarizations. Furthermore, the peak intensities for the two input polarizations are nearly comparable in terms of magnitude. Black silicon and porous silicon, both of which contain disordered nanowires, are examples of nanowires that emit light in response to polarisation variation. In contrast, the difference between s- and p-polarized light increased from 1.43 to 2.76 when the input was polarised in the p direction. In contrast, whereas either the positive or the negative input polarisation can excite the p-polarized output, only the positive or negative input can excite the s-polarized output. The

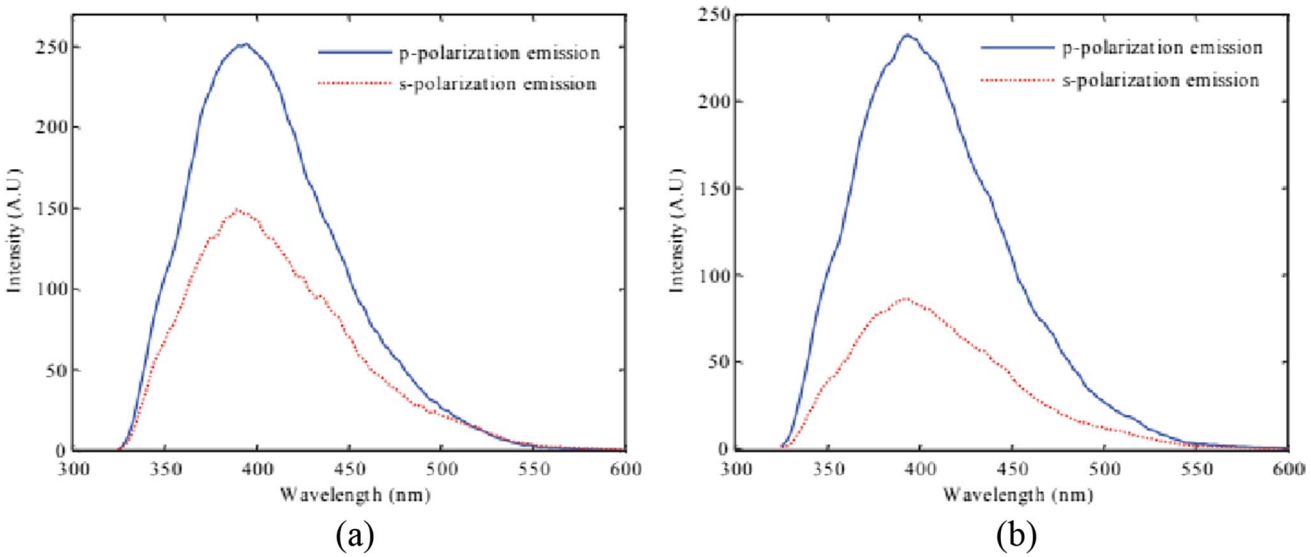

Fig. 16 (a) An ordered network of nanowires is activated by s-polarized input and produces polarization-resolved PL output. (b) When excited by p-polarized input, ordered nanowires provide polarization-resolved PL output

ratio between the two locations is 1.75:1 when comparing them peak to peak. As a result, s-polarized output has a PL memory due to this. It is conceivable to provide an explanation for the variation in the bending angles of the nanowires across the array.

The availability of several portable medical diagnostic gadgets, such as blood pressure monitors, glaucoma devices, and cholesterol sensors, pregnancy test sensors, heart rate monitors, and oxygen metres, has made diagnosis in the medical profession considerably easier in recent years. Gliomas are the most common and aggressive of all brain tumours, having a life expectancy of only a few months in the most severe form. Therapy planning is a crucial step in improving the quality of life of cancer patients. However, the massive amount of data generated by MRI makes manual segmentation impractical in a reasonable amount of time, limiting the use of precise quantitative measurements in clinical practise. Because there is so much variety in the spatial and anatomical features of brain tumours, an automatic and reliable segmentation approach is required. Even now researchers have worked on the various devices which can be helpful for bio-sensing applications [29–32].

7 Conclusion

The purpose of this work was to develop a platform based on silicon nanowires for future applications (SiNWs). According to this study, the simple MACE method for etching SiNs for different durations of etching time was demonstrated using 7 mg AgNO3 mass variation with 20 ml of water. We were able to characterise all of the different SiNs using a variety of techniques, including optical, structural, and morphological methods. The XRD technique was used to analyse the structural flaws and structural conformation of SiNs. The fabrication of high-anisotropy silicon nanowires was accomplished by the use of a top-down approach, electron beam lithography, and reactive ion etching. This method has allowed for the production of silicon nanowires with diameters lower than 15 nm for the first time in history. ZnO nanowires have been successfully generated on a number of different substrates. On the basis of diagrams, the process of ZnO nanowire formation has been described. In this study, researchers synthesised polycrystalline nanowires with diameters ranging from 20 to 100 nm, and lengths of only a few micrometres or less. These nanowies can be found in abundance across the substrate. The mechanical properties of nanowire thin films were investigated in detail. The ZnO nanowires that have been synthesised in situ are characterised by their softness and low hardness values. The polarisation resolved reflection technique was used to investigate and anticipate the light trapping properties of SiNWs. In a future laboratory study, nanowires coated with noble metals such as Ag or Au will boost Raman scattering from an array of SiNWs. Surface-enhanced Raman spectroscopy, for example, is one area where this could be advantageous. Further morphological properties of SiN were investigated using scanning electron microscopy. It was also able to determine the morphological properties of SiNs as a function of etching time using SEM data.

Acknowledgements The authors are thankful to Excel Engineering College, Namakkal, India for their cooperation and support during this research work.

Author Contributions A Mohamedyaseen, P Suresh Kumar: Conceptualization; A Mohamedyaseen, P Suresh Kumar: investigation; A Mohamedyaseen, P Suresh Kumar: resources; A Mohamedyaseen, P Suresh Kumar: data curation; A Mohamedyaseen, P Suresh Kumar: writing—original draft preparation; A Mohamedyaseen, P Suresh Kumar: writing—review and editing; A Mohamedyaseen, P Suresh Kumar: visualization; P Suresh Kumar: supervision.

Data Availability No supplementary materials.

Declarations

Consent to Participate Yes

Consent for Publication Author(s): A Mohamedyaseen

Conflict of Interest The authors declare that they have no conflict of interest.

Human and Animal Rights and Informed Consent This article does not contain any studies with human or animal subjects.

References

1. Campanelli RB, dos Santos MVP, da Cruz ASE, Pirota KR, Béron F (2021) Highly doped si single crystal nanowires via metallic flux nanonucleation. IEEE Trans Nanotechnol 20:739–743. https://doi.org/10.1109/TNANO.2021.3112905
2. Dwivedi P, Dhanekar S, Das S (2021) Near room temperature sensing by In_2O_3 decorated silicon nanowires for sensitive detection of ethanol. IEEE Sensors J 21(6):7275–7282. https://doi.org/10.1109/JSEN.2020.3046490
3. Yu Y, Chen S, Hu Q, Solomon P, Zhang Z (2021) Ultra-low noise schottky junction tri-gate silicon nanowire FET on bonded silicon-on-insulator substrate. IEEE Electron Device Lett 42(4):469–472. https://doi.org/10.1109/LED.2021.3057285
4. Salimi Kuchi P, Roshan H and Sheikhi MH (2020) A novel room temperature ethanol sensor based on PbS:SnS2 nanocomposite with enhanced ethanol sensing properties. J Alloys Compd 816:152666
5. Lai J, Su Y, Bu J, Li B, Li B, Zhang G (2020) Study on degradation mechanisms of thermal conductivity for confined nanochannel in gate-all-around silicon nanowire field-effect transistors. IEEE Trans Electron Devices 67(10):4060–4066. https://doi.org/10.1109/TED.2020.3014557
6. Nama Manjunatha K, Salaoru I, Milne WI, Paul S (2020) Comparative study of silicon nanowires grown from Ga, In, Sn, and

Bi for energy harvesting. IEEE J Photovoltaics 10(6):1667–1674. https://doi.org/10.1109/JPHOTOV.2020.3012628
7. Raine M et al (2019) SET sensitivity of trigate silicon nanowire field-effect transistors. IEEE Trans Nucl Sci 66(1):352–358. https://doi.org/10.1109/TNS.2018.2879194
8. Chen G et al (2019) Selective-assembling hybrid Porphyrin-Silicon Nanowire Field-Effect Transistor (PSNFET) for photonic sensor. IEEE Electron Device Lett 40(5):812–814. https://doi.org/10.1109/LED.2019.2903862
9. Yuan Z et al (2019) Sandwich-like composites of double-layer Co3O4 and reduced graphene oxide and their sensing properties to volatile organic compounds. J Alloys Compd 793:24–30
10. Hsin C, Wu M, Wang W (2019) Thermoelectric devices by half-millimeter-long silicon nanowires arrays. IEEE Trans Nanotechnol 18:921–924. https://doi.org/10.1109/TNANO.2019.2938624
11. Meng F et al (2019) Synthesis of Au nanoparticle-modified spindle shaped α-Fe2O3 nanorods and their gas sensing properties to Nbutanol. IEEE Trans Nanotechnol 18:911–920. https://doi.org/10.1109/TNANO.2019.2933569
12. Bhowmik B, Dutta K, Bhattacharyya P (2019) An efficient room temperature ethanol sensor device based on p-n homojunction of TiO2 nanostructures. IEEE Trans Electron Devices 66(2):1063–1068
13. Klüpfel FJ (2019) Influence of sacrificial layer germanium content on stacked-nanowire FET performance. IEEE Access 7:85855–85859. https://doi.org/10.1109/ACCESS.2019.2925201
14. Mohamed S, Shahada L, Swillam M (2018) Vertical silicon nanowires based directional coupler optical router. IEEE Photon Technol Lett 30(9):789–792. https://doi.org/10.1109/LPT.2018.2815040
15. Almoallem YD, Moghimi MJ, Jiang H (2018) Conformal antireflective surface formed onto 3-D silicon structure. J Microelectromech Syst 27(3):380–382. https://doi.org/10.1109/JMEMS.2018.2825649
16. Hayati L, Zare S, Lombardi F, Vittoria C (2018) Ferromagnetic resonance of Y3Fe5O12 nanowires. IEEE Magn Lett 9:1–4. https://doi.org/10.1109/LMAG.2018.2870055 (**4106204**)
17. Carnio BN, Elezzabi AY (2018) Second harmonic generation in CdSiP2 nanowires in the optical frequency regime. IEEE Photon Technol Lett 30(15):1408–1411. https://doi.org/10.1109/LPT.2018.2850519
18. Pregl S, Baraban L, Sessi V, Mikolajick T, Weber WM, Cuniberti G (2018) Signal and noise of Schottky-Junction parallel silicon nanowire transducers for biochemical sensing. IEEE Sensors J 18(3):967–975. https://doi.org/10.1109/JSEN.2017.2778188
19. Lai RA, Hymel TM, Narasimhan VK, Cui Y (2016) Schottky barrier catalysis mechanism in metal-assisted chemical etching of silicon. ACS Appl Mater Interfaces 8(14):8875–8879
20. Balderas-Valaez RF, Agarwaland V, Pacholski C (2016) Fabrication of porous silicon based optical sensors using metal assisted chemical etching. RSC Adv 6:21430
21. Kong L, Dasgupta B, Ren Yi, Mohseni PK, Hong M, Li X (2016) Wai Kin Chim & Sing Yang Chiam, evidences for redox reaction driven charge transfer and mass transport in metal-assisted chemical etching of silicon. Sci Rep 6:36582
22. Hashiguchi K, Suzuki K, Hiroshima H, Naitoh Y, Suga H (2018) Pt nanogap electrode fabrication by two-layer Lift-Off UV-NIL and nanowire breakdown. IEEE Trans Nanotechnol 17(6):1094–1097. https://doi.org/10.1109/TNANO.2018.2844125
23. Kamišalić A, Fister I, Turkanović M, Karakatič S (2018) Sensors and functionalities of non-invasive wrist-wearable devices: a review. Sensors 18(6):1714
24. Li M, Fan J, Xu X, Huang R (2017) Investigation on electrostatic discharge robustness of gate-all-around silicon nanowire transistors combined with thermal analysis. IEEE Electron Device Lett 38(12):1653–1656. https://doi.org/10.1109/LED.2017.2768484
25. Hazari A et al (2017) $1.3~\mu $ m Optical Interconnect on Silicon: A Monolithic III-Nitride Nanowire Photonic Integrated Circuit. IEEE J Quantum Electron 53(4):1–9. https://doi.org/10.1109/JQE.2017.2708526 (**6300109**)
26. Sohi PA, Kahrizi M (2017) Formation mechanism of silicon nanowires using chemical/electrochemical process. IEEE Trans Nanotechnol 16(3):507–513. https://doi.org/10.1109/TNANO.2017.2694428
27. Tanaka H, Suda J, Kimoto T (2017) Analysis of high-field hole transport in germanium and silicon nanowires based on boltzmann's transport equation. IEEE Trans Nanotechnol 16(1):118–125. https://doi.org/10.1109/TNANO.2016.2635110
28. Zhang S, Lou L, Gu YA (2017) Development of silicon nanowire-based nems absolute pressure sensor through surface micromachining. IEEE Electron Device Lett 38(5):653–656. https://doi.org/10.1109/LED.2017.2682500
29. Prakash MD, Nelam BG, Ahmadsaidulu S, Navaneetha A, Panigrahy AK (2021) Performance analysis of ion-sensitive field effect transistor with various oxide materials for biomedical applications. Silicon. https://doi.org/10.1007/s12633-021-01413-9
30. Prakash MD, Krsihna BV, Satyanarayana BVV, Vignesh NA, Panigrahy AK, Ahmadsaidulu S (2021) A study of an ultrasensitive label free silicon nanowire FET biosensor for cardiac troponin I detection. SILICON. https://doi.org/10.1007/s12633-021-01352-5
31. Meriga C, Ponnuri RT, Satyanarayana BVV, Gudivada AAK, Panigrahy AK and Prakash MD (2021) A novel teeth junction less gate all around FET for improving electrical characteristics. Silicon. https://doi.org/10.1007/s12633-021-00983-y
32. Sreenivasulu VB, Narendar V (2021) Junctionless gate-all-around nanowire FET with asymmetric spacer for continued scaling. Silicon. https://doi.org/10.1007/s12633-021-01471-z